Supporting Information

Multi-Functional Aramid Nanofiber/Carbon Nanotube Hybrid Aerogel Films

Peiying Hu[a,b†], *Jing Lyu*[b†], *Chen Fu*[b], *Wen-bin Gong*[b], *Jianhe Liao*[a], *Weibang Lu*[b], *Yongping Chen*[a]* *and Xuetong Zhang*[b,c]*

[a]Department of Polymer Materials and Engineering, School of Materials Science and Engineering, Hainan University, 58 Renmin Ave, Haikou, 570228, P. R. China

[b]Suzhou Institute of Nano-tech and Nano-bionics, Chinese Academy of Sciences, Suzhou 215123, P. R. China

[c]Department of Surgical Biotechnology, Division of Surgery & Interventional Science, University College London, London, NW3 2PF, UK

[†]These authors contributed equally to this work

[*]E-mail: chenyp@hainanu.edu.cn

[*]E-mail: xtzhang2013@sinano.ac.cn or xuetong.zhang@ucl.ac.uk

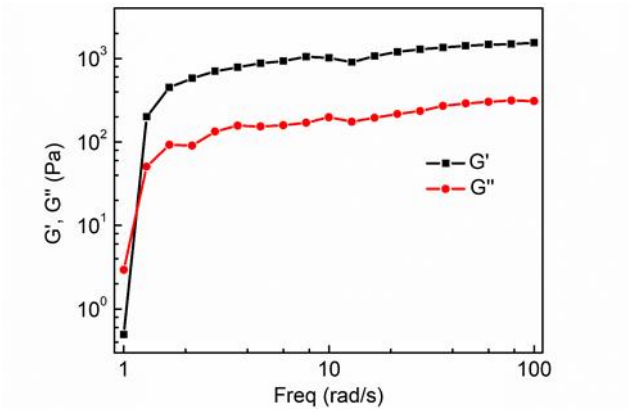

Figure S1. The rheological behaviors of ANF/CNT.

The rheological behaviors of ANF/CNT help us to confirm the sol-to-gel transition. The storage modulus (G′), characteristic of the elasticity of the ANF/CNT was lower than its loss modulus (G′′, referring to the viscosity) at initial stage, implying the sol state of ANF/CNT. Then the storage modulus increased rapidly and exceeded the loss modulus. The higher storage modulus than the corresponding loss modulus indicates the formation of gel. This sol-to-gel transition was attributed to the network structures formed rapidly between aramid nanofibers in the presence of water.

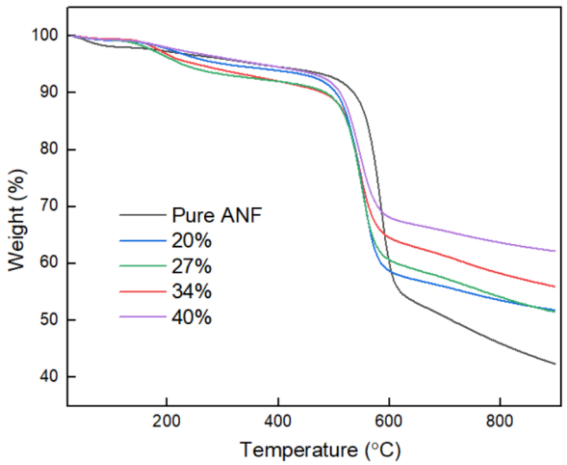

Figure S2. TGA curves of Pure ANF aerogel films and FC-ANF/CNT aerogel films with different CNT content.

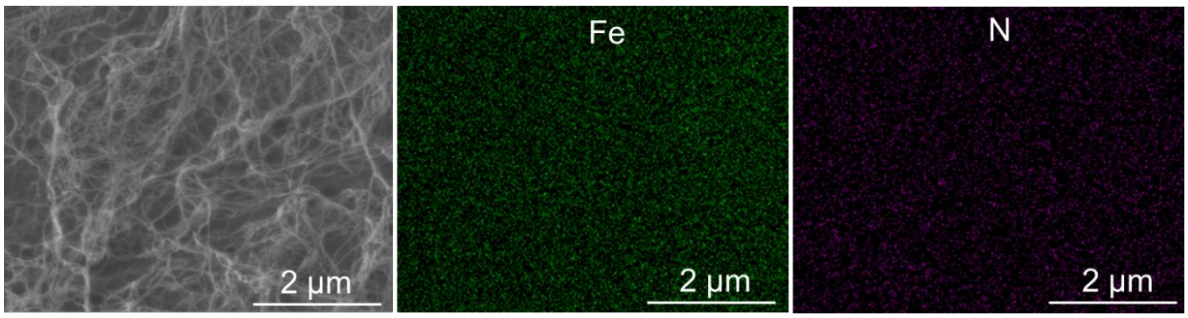

Figure S3. SEM image of the FC-ANF/CNT aerogel film and the corresponding EDS mapping.

It is difficult to distinguish between CNTs and ANFs in SEM images, since they are similar in diameter. In order to investigate the distribution of CNTs in ANFs matrix, pristine CNTs without acid treatment was mixed with ANFs, and subsequently was made into films for SEM and EDS observation. The iron (Fe) nanoparticles as catalyst in CNTs were distributed uniformly, confirming that CNTs were evenly distributed, without obvious agglomeration.

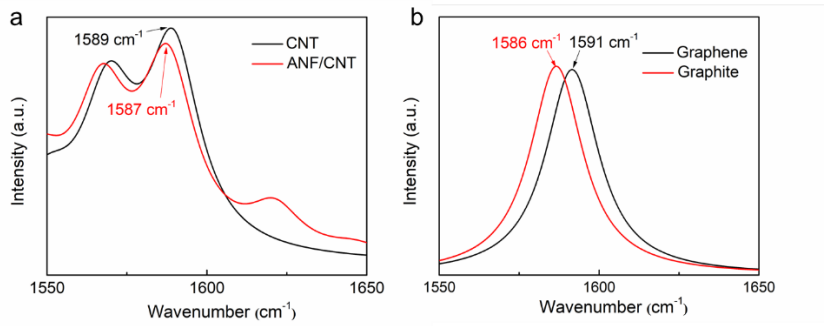

Figure S4. (a) The simulated Raman spectra of CNTs and ANFs/CNTs. (b) The simulated Raman spectra of monolayer graphene and graphite.

The Raman spectra were simulated based on density functional theory calculations by DMol3 package. All the calculations were carried out using Perdew–Burke–Ernzerhof (PBE) exchange-correlation functions in the framework of general gradient

approximation with all atoms fully relaxed. An all-electron double numerical basis set with polarization functions was used in this contribution. The convergence criteria applied for geometry optimizations were 2.0×10^{-5} au, 4.0×10^{-3} au $Å^{-1}$, and 5.0×10^{-3} Å for energy change, maximum force, and maximum displacement, respectively. The threshold for self-consistent-field density convergence was set to 1.0×10^{-5} eV. An aramid monomer laid on a large poly-aromatic hydrocarbon molecule of $C_{96}H_{24}$ was used to represent the π-π interactions between CNTs and ANFs in the experiments. The result shows that the Raman band shift is negligible (only about 2 cm^{-1}, as shown below), demonstrating that the contact points between entangled aramid nanofibers and CNTs are not massive, and those contacts are not enough to modify the Raman spectra.

To further investigate the π-π interactions between ANFs and CNTs, the graphite was modeled using a primitive cell with the in-plane and out-plane lattice parameters of 2.46 Å and 6.80 Å, respectively, for simplification. The π-π interactions between graphene sheets are relatively strong, but the simulation showed that the G band shift was only about 5 cm^{-1}. Therefore, the π-π interactions between aramid nanofibers and CNTs with very limited amount are not strong enough to modify the Raman spectra or improve the strength and Young's modulus of the hybrid aerogel films.

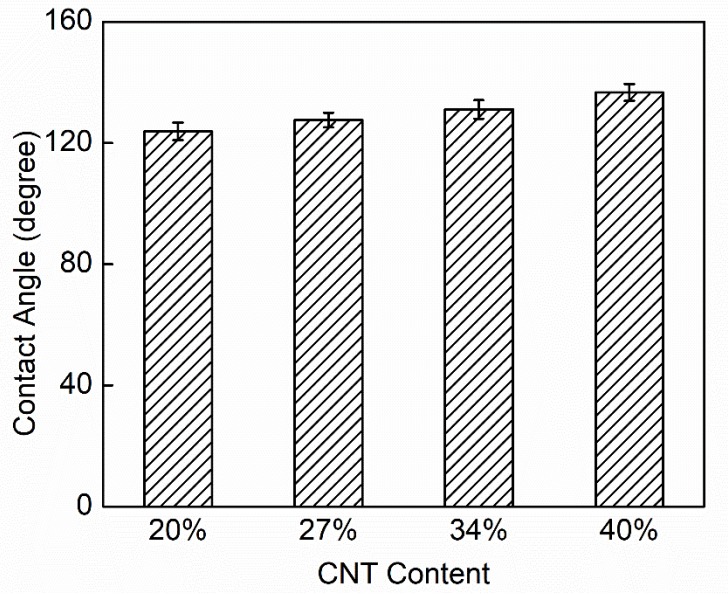

Figure S5. The contact angles of the FC-ANF/CNT aerogel films as a function of CNT contents.

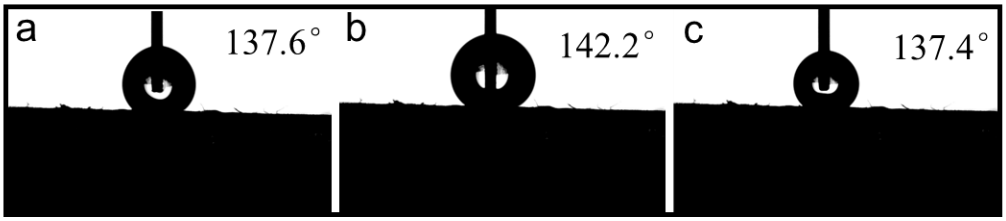

Figure S6. (a) Static contact angel, (b) forward angle and (c) backward angle of the FC-ANF/CNT.

To characterize the excellent hydrophobicity of the hybrid FC-ANF/CNT aerogel films, the forward and backward angles were tested by optical angle meter system. The static, forward and backward angle were 137.6°, 142.2° and 137.4°, respectively. The difference between the forward and backward angles is about 4.8°, indicating the excellent hydrophobicity.

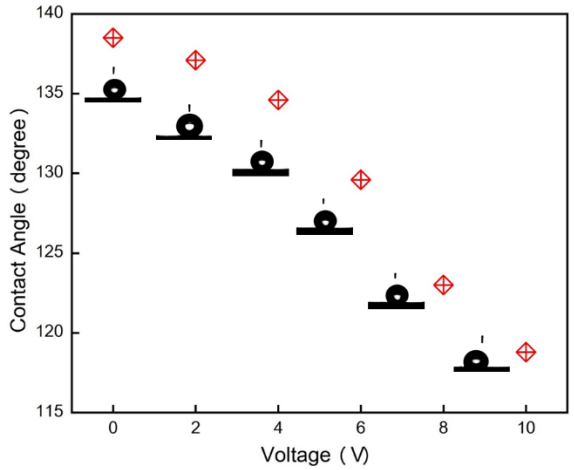

Figure S7. The contact angles of the FC-ANF/CNT as a function of applied voltages.

In order to investigate the hydrophobicity of the hybrid FC-ANF/CNT aerogel films under high temperature, 0 V-10 V voltage was applied to control the temperature of the aerogel film from room temperature to 80 °C. The contact angle decreased with the increase of film temperatures, but the film remains nonwetting (118°), even at 80 °C.

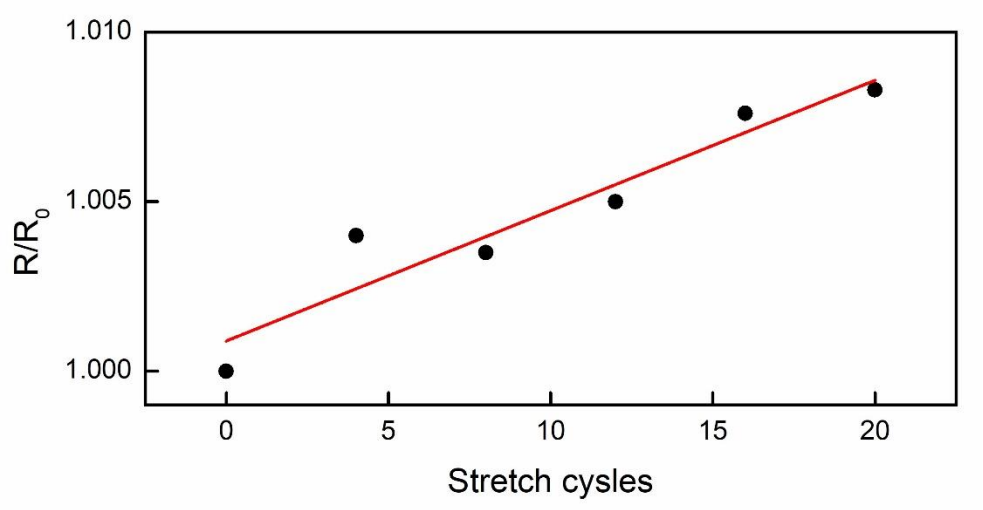

Figure S8. The relative electrical resistance (R/R_0) of FC-ANF/CNT aerogel films under cyclic tensile test.

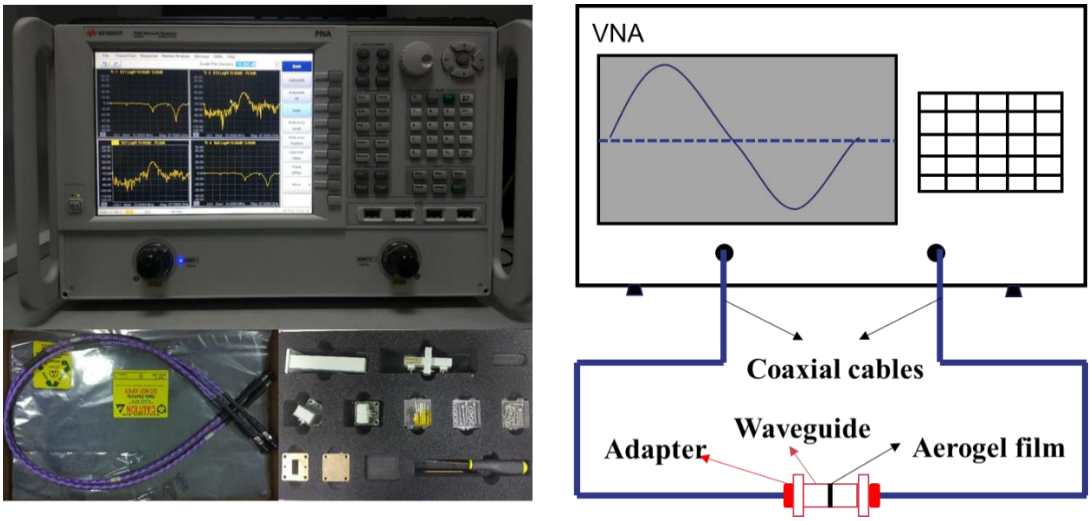

Figure S9. Physical diagram and schematic diagram of Vector network analyzer

The total EMI shielding performance can be described by three major mechanisms, namely, microwave reflection loss, multiple internal reflection effectiveness, and microwave absorption loss. It should be mentioned that the multiple internal reflection is always considered as an absorption because electromagnetic waves reflect back-and-forth until absorbed or dissipated as heat.

$$R=\left|S_{11}\right|^2, T=\left|S_{21}\right|^2, A=1-R-T \quad (1)$$

$$\text{EMI SE}_T=-10\ \lg\left(\frac{P_t}{P_i}\right)=-10\ \lg\left|S_{21}\right|^2=-10\ \lg(T) \quad (2)$$

$$\text{EMI SE}_\text{T}=\text{SE}_\text{A}+\text{SE}_\text{R}+\text{SE}_\text{M} \quad (3)$$

$$\text{SE}_A=-10\ \lg\left(\frac{T}{1-R}\right) \quad (4)$$

$$\text{SE}_R=-10\ \lg(1-R) \quad (5)$$

where $|S_{ij}|$ represents the power transmitted from port i to port j; R, A, T are the reflection coefficient, absorption coefficient, and transmission coefficient, respectively; SE_T, SE_R and SE_A are the total shielding effectiveness, reflection effectiveness, and absorption effectiveness, respectively; P_i is the incident power and P_t is the transmitted power.

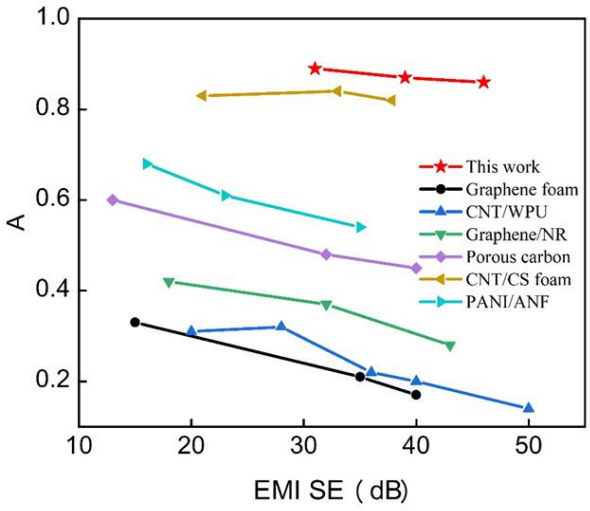

Figure S10. Comparison the absorption ratio of total shielding efficiency of the FC-ANF/CNT with other shielding materials.[1–6]

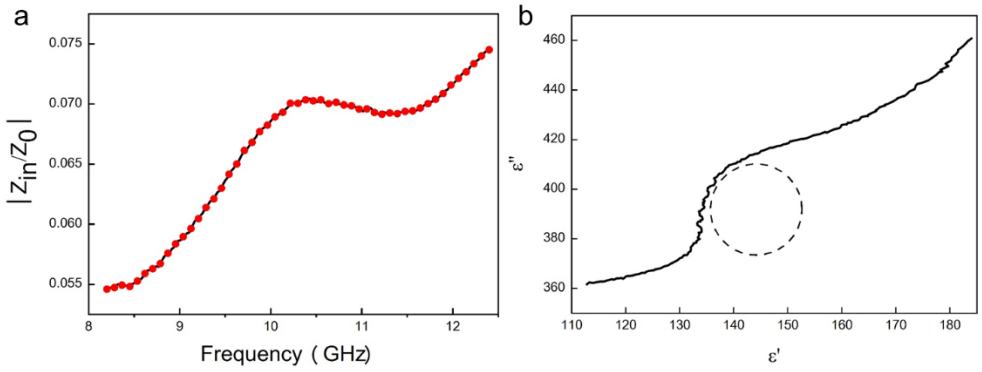

Figure S11. (a) The modulus of the normalized characteristic impedance (Z_{in}/Z_0) curve and (b) the ε'- ε'' curve of the FC-ANF/CNT.

Electromagnetic parameters are usually used to analysis the mechanism of microwave absorption. According to the transmission theory, the reflection of microwave on the surface of absorb materials is related to the impedance match, which is usually characterized by the ratio of the impedance of electromagnetism in the absorber (Z_{in}) and free space (Z_0).

$$Z_{in} = Z_0 \frac{1+R}{1-R} \tag{6}$$

$$Z_{in} = Z_0\sqrt{\mu_r/\varepsilon_r}\tanh[j(2\pi fd/c)\sqrt{\mu_r\varepsilon_r}] \tag{7}$$

R is the reflection coefficient, which can be expression by the following equation.

$$R = \frac{Z_{in}-Z_0}{Z_{in}+Z_0} = \frac{\frac{Z_{in}}{Z_0}-1}{\frac{Z_{in}}{Z_0}+1} \tag{8}$$

From equation (8), when the value of Z_{in}/Z_0 is 1, the value of *R* is 0, means no reflection occurs on the surface of absorb material which shows the perfect impedance matching. As shown in Figure S10a, the value of Z_{in}/Z_0 is less than 1, indicating imperfect impedance matching resulting in inevitable reflection.

Debye dielectric relaxation model was adopted to investigate the mechanisms of the permittivity dispersion. According to Debye theory, the relationship between ε' and ε'' can be described as:

$$\left(\varepsilon' - \frac{\varepsilon_s - \varepsilon_\infty}{2}\right)^2 + (\varepsilon'')^2 = \left(\frac{\varepsilon_s - \varepsilon_\infty}{2}\right)^2 \tag{9}$$

where, ε' and ε'' are the real part and imaginary part of relative permittivity; ε_s and ε_∞ are static permittivity and relative dielectric permittivity at high frequency limit, respectively. The curve of ε' and ε'' would be a semicircle, which stands for a Debye relaxation process. In Figure S10b, two lines can be found in the curve of real and imaginary parts of the permittivity, corresponding to the conductance loss. The existing circle relationship of real and imaginary parts of permittivity is attributed to the polarization relaxation loss.

Table S1. EMI shielding performance of this work in comparison to that of other shielding materials reported in the literature.

Materials	Thickness (mm)	EMI SE (dB)	Reference
S-doped r-GO	0.15	38.5	[7]
rGO/Fe_3O_4	0.25	24.0	[8]
rGO/Fe_2O_3/PVA	0.36	20.3	[9]
CNT/PPS	1.5	43.0	[10]
rGO/PI	0.8	21.0	[11]
CNT/PS	1.0	19.3	[12]
Ni fiber/PES	2.85	58.0	[13]
PEDOT:PSS/Graphite	0.8	70.0	[14]
$Ti_3C_2T_X$	1.0	70.6	[15]
PEDOT/CNT	2.85	58.0	[16]
PANI/CNT	2.4	31.5	[17]
PANI/GS	2.4	34.2	[17]
Graphene Foam	1.6	20.0	[18]
SWCNT/PU	2.0	17.0	[19]
rGO/C	5.0	38.0	[20]
Cellulose/Graphene	5.0	47.8	[21]
CNT-C/SiC	3.0	48.0	[22]
rGO/CF/Fe_2O_3	0.4	42.0	[23]
FC-ANF/CNT	**0.568**	**41.9**	**This work**
FC-ANF/CNT	**0.396**	**35.6**	**This work**
FC-ANF/CNT	**0.276**	**27.8**	**This work**
FC-ANF/CNT	**0.168**	**22.7**	**This work**

Specific EMI SE (SSE) can be calculated by dividing the EMI SE with the density of the material as:

$$\mathrm{SSE} = \frac{EMI\ \ SE}{\rho} \tag{10}$$

The following equation is used to evaluate the thickness-specific EMI SE (SSE/t) of a material.

$$\mathrm{SSE/t} = \frac{EMI\ \ SE}{\rho \cdot t} \tag{11}$$

Table S2. EMI shielding performance of this work in terms of thickness-specific EMI SE in comparison to that of other shielding materials.

Materials	Thickness (mm)	Density ($mg \cdot cm^{-3}$)	EMI SE (dB)	SSE/t ($dB \cdot cm^2 \cdot g^{-1}$)	Reference
G/PEDOT:PSS	1.5	22	69.1	20827.0	[24]
G/PEDOT:PSS	1.5	76.2	69.1	8040.0	[24]
Graphene foam	2.0	14.0	64.4	11500.0	[25]
CNT/CS	4.0	17.6	37.6	8556.0	[5]
C-CNT/CNF	5.0	14.0	21.0	3370.0	[26]
PEI/Graphene	2.3	30.0	22.0	3190.0	[27]
Graphene	1.0	40.0	20	5000.0	[18]
CNT/cellulose foam	2.5	32.3	50.8	6287.0	[28]
CNT/WPU	2.3	9.0	21.7	10483.0	[29]
rGO/PI	0.8	22.0	21.0	11712.0	[11]
Ag nanowire/WPU	2.3	45.0	64.0	6183.0	[30]
Cellulose/CNT	2.5	77.0	40.0	2080.0	[31]
Graphene/PDMS	3.0	60.0	36.0	2000.0	[18]

G/CNTs	1.6	97.1	36	2317.2	[32]
G/CNTs/PDMS	2.0	90.0	75.0	4165.0	[33]
TiO_2/SiO_2@PPy@rGO	0.24	89.0	30.0	13829.0	[34]
cotton-derived carbon	0.3	60.0	46.9	26055.0	[35]
cotton-derived carbon	0.3	100.0	41.7	13900.0	[35]
cotton-derived carbon	0.3	130.0	33.7	8641.0	[35]
cotton-derived carbon	0.3	140.0	26.9	6405.0	[35]
CNT/PDMS	1.8	10.0	54.8	5480.0	[36]
$Ti_3C_2T_x$ aerogel film	0.013	2780	46.2	13195	[37]
$Ti_3C_2T_x$/SA aerogel	0.014	2500	43.9	14830	[37]
$Ti_3C_2T_x$/CA aerogel	0.026	1350	54.3	17586	[37]
Graphene aerogel-like films	0.12	410	70-105	16000-21000	[38]
MXene Foams	0.006	390	32	136752	[39]
MXene Foams	0.018	400	50	69444	[39]
MXene Foams	0.060	220	70	53030	[39]
FC-ANF/CNT	**0.568**	**40.3**	**41.9**	**18304.6**	**This work**
FC-ANF/CNT	**0.396**	**40.3**	**35.6**	**22307.4**	**This work**
FC-ANF/CNT	**0.276**	**40.3**	**27.8**	**24993.7**	**This work**
FC-ANF/CNT	**0.168**	**40.3**	**22.7**	**33528.3**	**This work**

REFERENCES

(1) Li, Y.; Zhang, H.-B.; Zhang, L.; Shen, B.; Zhai, W.; Yu, Z.-Z.; Zheng, W. One-Pot Sintering Strategy for Efficient Fabrication of High-Performance and Multifunctional Graphene Foams. *ACS Appl. Mater. Interfaces* **2017**, *9*, 13323–

13330.

(2) Chem, J. M.; Liu, Q.; Gu, J.; Zhang, W.; Miyamoto, Y.; Zhang, D. Biomorphic Porous Graphitic Carbon for Electromagnetic Interference Shielding. *J. Mater. Chem.* **2012**, *22*, 21183–21188.

(3) Zeng, Z.; Jin, H.; Chen, M.; Li, W.; Zhou, L.; Zhang, Z. Lightweight and Anisotropic Porous MWCNT/WPU Composites for Ultrahigh Performance Electromagnetic Interference Shielding. *Adv. Funct. Mater.* **2016**, *26*, 303–310.

(4) Jia, L.-C.; Yan, D.-X.; Yang, Y.; Zhou, D.; Cui, C.-H.; Bianco, E.; Lou, J.; Vajtai, R.; Li, B.; Ajayan, P. M.; Li, Z.-M. High Strain Tolerant EMI Shielding Using Carbon Nanotube Network Stabilized Rubber Composite. *Adv. Mater. Technol.* **2017**, *2*, 1700078.

(5) Li, M.-Z.; Jia, L.-C.; Zhang, X.-P.; Yan, D.-X.; Zhang, Q.-C.; Li, Z.-M. Robust Carbon Nanotube Foam for Efficient Electromagnetic Interference Shielding and Microwave Absorption. *J. Colloid Interface Sci.* **2018**, *530*, 113–119.

(6) Lyu, J.; Zhao, X.; Hou, X.; Zhang, Y.; Li, T.; Yan, Y. Electromagnetic Interference Shielding Based on a High Strength Polyaniline-Aramid Nanocomposite. *Compos. Sci. Technol.* **2017**, *149*, 159–165.

(7) Shahzad, F.; Kumar, P.; Kim, Y.-H.; Hong, S. M.; Koo, C. M. Biomass-Derived Thermally Annealed Interconnected Sulfur-Doped Graphene as a Shield against Electromagnetic Interference. *ACS Appl. Mater. Interfaces* **2016**, *8*, 9361–9369.

(8) Song, W.-L.; Guan, X.-T.; Fan, L.-Z.; Cao, W.-Q.; Wang, C.-Y.; Zhao, Q.-L.; Cao, M.-S. Magnetic and Conductive Graphene Papers toward Thin Layers of Effective Electromagnetic Shielding. *J. Mater. Chem. A* **2015**, *3*, 2097–2107.

(9) Yuan, B.; Bao, C.; Qian, X.; Song, L.; Tai, Q.; Liew, K. M.; Hu, Y. Design of Artificial Nacre-like Hybrid Films as Shielding to Mitigate Electromagnetic Pollution. *Carbon* **2014**, *75*, 178–189.

(10) Zhang, X.-P.; Jia, L.-C.; Zhang, G.; Yan, D.-X.; Li, Z.-M. A Highly Efficient and Heat-Resistant Electromagnetic Interference Shielding Carbon Nanotube/Poly(Phenylene Sulfide) Composite via Sinter Molding. *J. Mater. Chem. C* **2018**, *6*, 10760–10766.

(11) Li, Y.; Pei, X.; Shen, B.; Zhai, W.; Zhang, L.; Zheng, W. Polyimide/Graphene Composite Foam Sheets with Ultrahigh Thermostability for Electromagnetic Interference Shielding. *RSC Adv.* **2015**, *5*, 24342–24351.

(12) Yang, Y.; Gupta, M. C.; Dudley, K. L.; Lawrence, R. W. Novel Carbon Nanotube−Polystyrene Foam Composites for Electromagnetic Interference Shielding. *Nano Lett.* **2005**, *5*, 2131–2134.

(13) Shui, X.; Chung, D. D. L. Nickel Filament Polymer-Matrix Composites with Low Surface Impedance and High Electromagnetic Interference Shielding Effectiveness. *J. Electron. Mater.* **2000**, *26*, 928–934.

(14) Agnihotri, N.; Chakrabarti, K.; De, A. Highly Efficient Electromagnetic

Interference Shielding Using Graphite Nanoplatelet/Poly(3,4-Ethylenedioxythiophene)–Poly(Styrenesulfonate) Composites with Enhanced Thermal Conductivity. *RSC Adv.* **2015**, *5*, 43765–43771.

(15) Han, M.; Yin, X.; Hantanasirisakul, K.; Li, X.; Iqbal, A.; Hatter, C. B.; Anasori, B.; Koo, C. M.; Torita, T.; Soda, Y.; Zhang, L.; Cheng, L.; Gogotsi, Y. Anisotropic MXene Aerogels with a Mechanically Tunable Ratio of Electromagnetic Wave Reflection to Absorption. *Adv. Opt. Mater.* **2019**, *7*, 1900267.

(16) Farukh, M.; Pratap, A.; Dhawan, S. K. Enhanced Electromagnetic Shielding Behavior of Multi-Walled Carbon Nanotube Entrenched Poly(3,4-Ethylenedioxythiophene) Nanocomposites. *Compos. Sci. Technol.* **2015**, *114*, 94–102.

(17) Yuan, B.; Yu, L.; Sheng, L.; An, K.; Zhao, X. Comparison of Electromagnetic Interference Shielding Properties between Single-Wall Carbon Nanotube and Graphene Sheet/Polyaniline Composites. *J. Phys. D: Appl. Phys.* **2012**, *45*, 235108.

(18) Chen, Z.; Xu, C.; Ma, C.; Ren, W.; Cheng, H. M. Lightweight and Flexible Graphene Foam Composites for High-Performance Electromagnetic Interference Shielding. *Adv. Mater.* **2013**, *25*, 1296–1300.

(19) Liu, Z.; Bai, G.; Huang, Y.; Ma, Y.; Du, F.; Li, F.; Guo, T.; Chen, Y. Reflection and Absorption Contributions to the Electromagnetic Interference Shielding of

Single-Walled Carbon Nanotube/Polyurethane Composites. *Carbon* **2007**, *45*, 821–827.

(20) Narasimman, R. Graphene-Reinforced Carbon Composite Foams with Improved Strength and EMI Shielding from Sucrose and Graphene Oxide. *J. Mater. Sci.* **2015**, *50*, 8018–8028.

(21) Wan, Y.-J.; Zhu, P.-L.; Yu, S.-H.; Sun, R.; Wong, C.-P.; Liao, W.-H. Ultralight, Super-Elastic and Volume-Preserving Cellulose Fiber/Graphene Aerogel for High-Performance Electromagnetic Interference Shielding. *Carbon* **2017**, *115*, 629–639.

(22) Mei, H.; Han, D.; Xiao, S.; Ji, T.; Tang, J.; Cheng, L. Improvement of the Electromagnetic Shielding Properties of C/SiC Composites by Electrophoretic Deposition of Carbon Nanotube on Carbon Fibers. *Carbon* **2016**, *109*, 149–153.

(23) Singh, A. P.; Garg, P.; Alam, F.; Singh, K.; Mathur, R. B.; Tandon, R. P.; Chandra, A.; Dhawan, S. K. Phenolic Resin-Based Composite Sheets Filled with Mixtures of Reduced Graphene Oxide, γ-Fe2O3 and Carbon Fibers for Excellent Electromagnetic Interference Shielding in the X-Band. *Carbon* **2012**, *50*, 3868–3875.

(24) Wu, Y.; Wang, Z.; Liu, X.; Shen, X.; Zheng, Q.; Xue, Q.; Kim, J.-K. Ultralight Graphene Foam/Conductive Polymer Composites for Exceptional Electromagnetic Interference Shielding. *ACS Appl. Mater. Interfaces* **2017**, *9*, 9059–9069.

(25) Zhang, Y.; Huang, Y.; Zhang, T.; Chang, H.; Xiao, P.; Chen, H.; Huang, Z.; Chen, Y. Broadband and Tunable High-Performance Microwave Absorption of an Ultralight and Highly Compressible Graphene Foam. *Adv. Mater.* **2015**, *27*, 2049–2053.

(26) Pitkänen, O.; Tolvanen, J.; Szenti, I.; Kukovecz, Á.; Hannu, J.; Jantunen, H.; Kordas, K. Lightweight Hierarchical Carbon Nanocomposites with Highly Efficient and Tunable Electromagnetic Interference Shielding Properties. *ACS Appl. Mater. Interfaces* **2019**, *11*, 19331–19338.

(27) Ling, J.; Zhai, W.; Feng, W.; Shen, B.; Zhang, J.; Zheng, W. ge. Facile Preparation of Lightweight Microcellular Polyetherimide/Graphene Composite Foams for Electromagnetic Interference Shielding. *ACS Appl. Mater. Interfaces* **2013**, *5*, 2677–2684.

(28) Huang, H.-D.; Liu, C.-Y.; Zhou, D.; Jiang, X.; Zhong, G.-J.; Yan, D.-X.; Li, Z.-M. Cellulose Composite Aerogel for Highly Efficient Electromagnetic Interference Shielding. *J. Mater. Chem. A* **2015**, *3*, 4983–4991.

(29) Zeng, Z.; Jin, H.; Chen, M.; Li, W.; Zhou, L.; Xue, X.; Zhang, Z. Microstructure Design of Lightweight, Flexible, and High Electromagnetic Shielding Porous Multiwalled Carbon Nanotube/Polymer Composites. *Small* **2017**, *13*, 1701388.

(30) Zeng, Z.; Chen, M.; Pei, Y.; Seyed Shahabadi, S. I.; Che, B.; Wang, P.; Lu, X. Ultralight and Flexible Polyurethane/Silver Nanowire Nanocomposites with Unidirectional Pores for Highly Effective Electromagnetic Shielding. *ACS Appl.*

Mater. Interfaces **2017**, *9*, 32211–32219.

(31) Li, X.-H.; Li, X.; Liao, K.-N.; Min, P.; Liu, T.; Dasari, A.; Yu, Z.-Z. Thermally Annealed Anisotropic Graphene Aerogels and Their Electrically Conductive Epoxy Composites with Excellent Electromagnetic Interference Shielding Efficiencies. *ACS Appl. Mater. Interfaces* **2016**, *8*, 33230–33239.

(32) Kong, L.; Yin, X.; Han, M.; Yuan, X.; Hou, Z.; Ye, F.; Zhang, L.; Cheng, L.; Xu, Z.; Huang, J. Macroscopic Bioinspired Graphene Sponge Modified with In-Situ Grown Carbon Nanowires and Its Electromagnetic Properties. *Carbon* **2017**, *111*, 94–102.

(33) Sun, X.; Liu, X.; Shen, X.; Wu, Y.; Wang, Z.; Kim, J.-K. Reprint of Graphene Foam/Carbon Nanotube/Poly(Dimethyl Siloxane) Composites for Exceptional Microwave Shielding. *Composites, Part A* **2017**, *92*, 190–197.

(34) Huang, L.; Li, J.; Li, Y.; He, X.; Yuan, Y. Lightweight and Flexible Hybrid Film Based on Delicate Design of Electrospun Nanofibers for High-Performance Electromagnetic Interference Shielding. *Nanoscale* **2019**, *11*, 8616–8625.

(35) Ma, X.; Li, Y.; Shen, B.; Zhang, L.; Chen, Z.; Liu, Y.; Zhai, W.; Zheng, W. Carbon Composite Networks with Ultrathin Skin Layers of Graphene Film for Exceptional Electromagnetic Interference Shielding. *ACS Appl. Mater. Interfaces* **2018**, *10*, 38255–38263.

(36) Lu, D.; Mo, Z.; Liang, B.; Yang, L.; He, Z.; Zhu, H.; Tang, Z.; Gui, X. Flexible,

Lightweight Carbon Nanotube Sponges and Composites for High-Performance Electromagnetic Interference Shielding. *Carbon* **2018**, *133*, 457–463.

(37) Zhou, Z.; Liu, J.; Zhang, X.; Tian, D.; Zhan, Z.; Lu, C. Ultrathin MXene/Calcium Alginate Aerogel Film for High-Performance Electromagnetic Interference Shielding. *Adv. Mater. Interfaces* **2019**, *6*, 1802040.

(38) Xi, J.; Li, Y.; Zhou, E.; Liu, Y.; Gao, W.; Guo, Y.; Ying, J.; Chen, Z.; Chen, G.; Gao, C. Graphene Aerogel Films with Expansion Enhancement Effect of High-Performance Electromagnetic Interference Shielding. *Carbon* **2018**, *135*, 44–51.

(39) Liu, J.; Zhang, H.-B.; Sun, R.; Liu, Y.; Liu, Z.; Zhou, A.; Yu, Z.-Z. Hydrophobic, Flexible, and Lightweight MXene Foams for High-Performance Electromagnetic-Interference Shielding. *Adv. Mater.* **2017**, *29*, 1702367.